Magnetic reconnection and hot-spot formation in black-hole accretion disks

Bart Ripperda,[1,2,*] Fabio Bacchini,[3] and Alexander A. Philippov[1]

[1] *Center for Computational Astrophysics, Flatiron Institute, 162 Fifth Avenue, New York, NY 10010, USA*
[2] *Department of Astrophysical Sciences, Peyton Hall, Princeton University, Princeton, NJ 08544, USA*
[3] *Centre for mathematical Plasma Astrophysics, Department of Mathematics, Katholieke Universiteit Leuven, Celestijnenlaan 200B, B-3001 Leuven, Belgium*

(Received January 30, 2020; Revised January 30, 2020; Accepted March 11, 2020)

Submitted to ApJ

ArXiv:2003.04330, 9 Mar 2020

Miljenko Čemeljić, SHAO, Visiting Scientist (PIFI)

Miljenko Čemeljić

席門傑

Μιλιενκο Τσεμεγλιτς

[PIFI Visiting Scientist,
Shanghai Astronomical Observatory,
Chinese Academy of Sciences]

Office: 1607 (Shanghai)
Email: miki at shao.ca.cn
Phone: +86-21-34775332

[Nicolaus Copernicus Astronomical Center, Warsaw, Poland]

Office: 139 (Warsaw)
Email: miki at camk.edu.pl
Phone: +48-22-3296139

[Visiting Scholar, Academia Sinica
Institute of Astronomy and Astrophysics
Taipei, Taiwan]

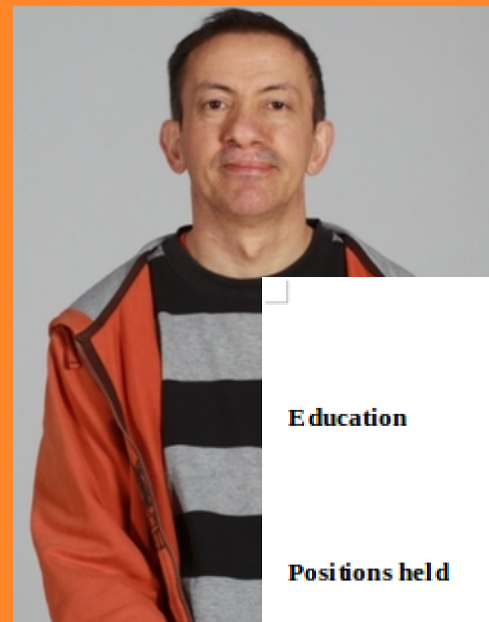

Curriculum vitae – Miljenko Čemeljić

April 2020

Education

: University of Potsdam, Germany, PhD in Astrophysics, January 2005
: University of Zagreb, Croatia, Faculty of Science, Diplom in Physics, April 1996

Positions held

: **Visiting Scientist** (PIFI), Shanghai Observatory, CAS, Jan 2020-
: **Visiting Scholar**, Academia Sinica, Taipei, Taiwan, Jun 2019-
: **Assistant Researcher**, Nicolaus Copernicus Astronomical Center, Polish Academy of Sciences, Warsaw, Poland, Sep 2018-
: Postdoctoral Researcher, Nicolaus Copernicus Astronomical Center, Polish Academy of Sciences, Warsaw, Poland, Oct 2015-Aug 2018
: Postdoctoral Researcher, CEA Saclay, LDEE/Sap, Paris, France, Jun 2014-Sep 2015
: **TIARA Visiting Scholar**, ASIAA, Academia Sinica, Taipei, Taiwan, Aug 2009-May 2014
: Visiting Researcher, IASA & University of Athens, Greece, Feb 2009-Jun 2009
: Visiting Lecturer, University of Split, Croatia, Dec 2008
: **TIARA Visiting Scholar**, ASIAA, Academia Sinica, Hsinchu, Taiwan, Feb 2007-Dec 2008
: **Marie Curie RTN Senior Postdoctoral Fellow**, "JETSET", IASA & University of Athens, Greece, Oct 2005-Feb 2007
: TIARA Postdoctoral Fellow, ASIAA, Academia Sinica, Hsinchu, Taiwan, Mar 2005-Sep 2005
: PhD student, Astrophysikalisches Institut Potsdam, Dec 1999–Jul 2003
: Research Assistant, Polish Academy of Science, Nicolaus Copernicus Astronomical Center, Warsaw, Poland, Dec 1995-Jun 1996; Jan 1997–Jun 1999

Croatia, Island of Pag

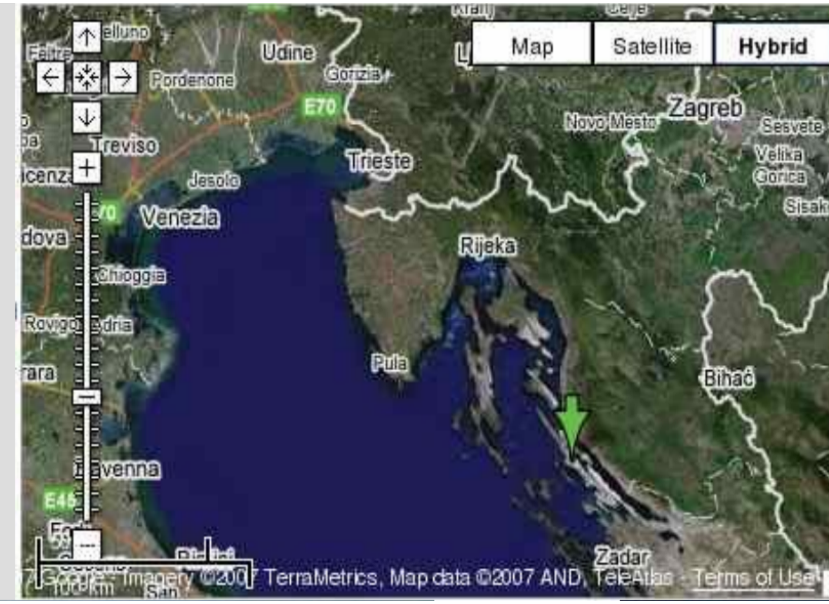

Magnetic reconnection and hot-spot formation in black-hole accretion disks

Bart Ripperda,[1,2,*] Fabio Bacchini,[3] and Alexander A. Philippov[1]

[1] *Center for Computational Astrophysics, Flatiron Institute, 162 Fifth Avenue, New York, NY 10010, USA*
[2] *Department of Astrophysical Sciences, Peyton Hall, Princeton University, Princeton, NJ 08544, USA*
[3] *Centre for mathematical Plasma Astrophysics, Department of Mathematics, Katholieke Universiteit Leuven, Celestijnenlaan 200B, B-3001 Leuven, Belgium*

(Received January 30, 2020; Revised January 30, 2020; Accepted March 11, 2020)

Submitted to ApJ

ArXiv:2003.04330, 9 Mar 2020

Outline

- Observations
- Numerical simulations-reconnection
- Toy model: Orszag & Tang vortex
- Reconnection rate
- Reconnection in BH accretion flows
- Simulations-setup (SANE, MAD)
- Simulation-results
- Summary

Observations-episodic flares from Sgr A*

-Bright, coincident episodic X-ray and near-infrared flares are detected on roughly a daily basis coming from Sgr A* , the supermassive black hole in the center of our Galaxy.

-Their origin is generally associated with electron acceleration in a localized flaring region not larger than a few gravitational radii rather than with a global increase in the accretion rate or jet power.

-The gravity Collaboration (2018) reported detection of positional changes of such near-infrared flares originating from within 10 gravitational radii of the black hole. The observed variable emission is probably due to the motion of a compact “hot spot” orbiting within a dynamical time scale of the compact object.

Numerical simulations-reconnection

-axisymmetric general-relativistic resistive magnetohydrodynamics (GRRMHD) simulations to model magnetic reconnection and associated plasmoid formation in a wide range of accretion flows. (with Black Hole Accretion Code BHAC, Porth et al. 2017; Olivares et al. 2019, using the AMR and numerical viscosity [caveat, as magnetic Prandtl number Pm~viscosity/resistivity~1])

Since magnetic reconnection plays important role, quantify of its effect is important.

There are (too)many publications since the first mentioning of reconnection in the solar physics context by Giovanelli (1946). There is still no definitive description.

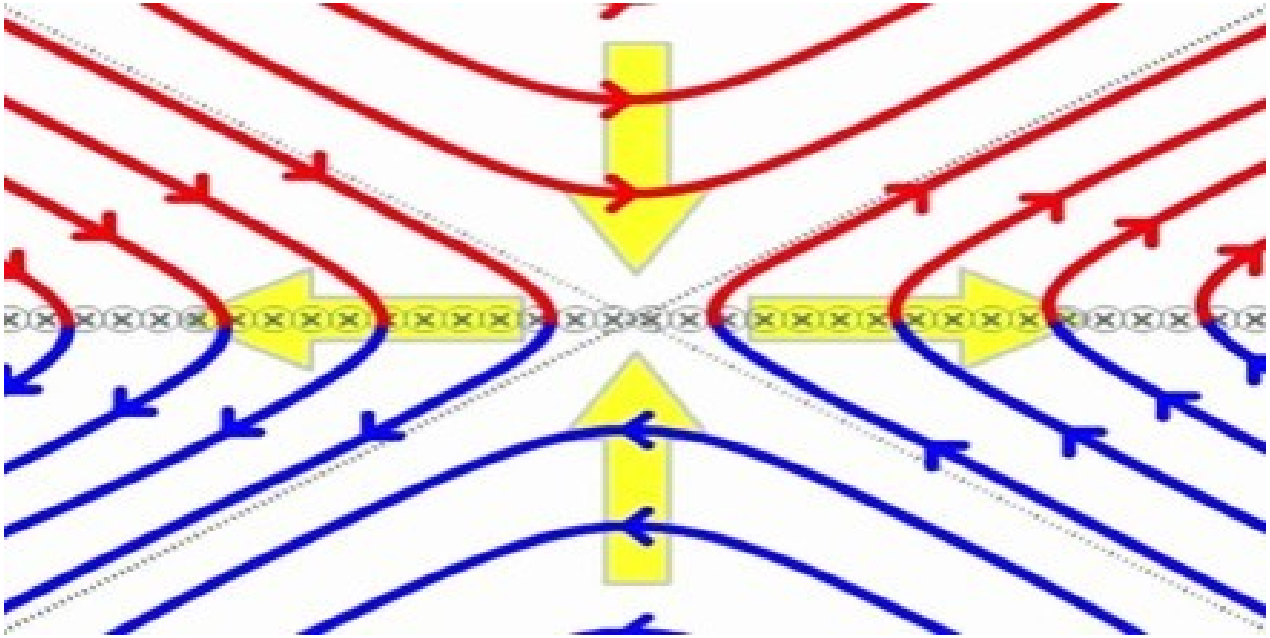

Numerical simulations-reconnection

PHYSICS OF PLASMAS **21**, 032121 (2014)

Magnetic reconnection in a comparison of topology and helicities in two and three dimensional resistive magnetohydrodynamic simulations

M. Čemeljić[a] and R.-Y. Huang[b]
Academia Sinica, Institute of Astronomy and Astrophysics and Theoretical Institute for Advanced Research in Astrophysics, P.O. Box 23-141, Taipei 106, Taiwan

(Received 26 December 2013; accepted 12 March 2014; published online 24 March 2014)

Through a direct comparison between numerical simulations in two and three dimensions, we investigate topological effects in reconnection. A simple estimate on increase in reconnection

Harris current sheet is formed initially with magnetic field which is parallel to the Y axis and is varying in the X direction:

$$\mathbf{B_2}(x) = \mathbf{y}B_0 \tanh(\mathbf{x}/b)$$

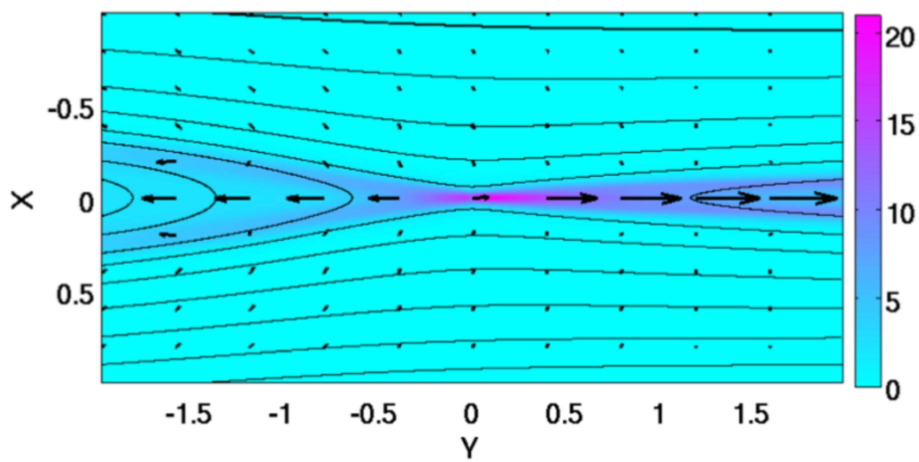

FIG. 2. Reconnection in two dimensions at T = 30 in code units, with current density shown in color grading, magnetic field contour lines in solid lines, and arrows showing velocity.

Numerical simulations-reconnection

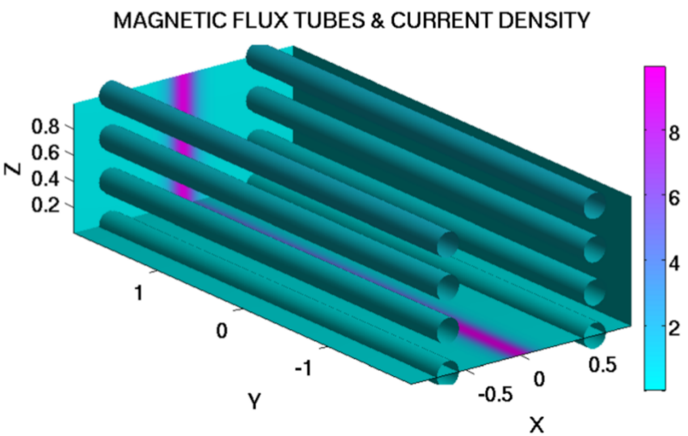

FIG. 1. Setup of initial and boundary conditions in our simulations in three dimensions. In two dimensional simulations, Z = 0. Color grading is showing a current density in code units, at the boundary planes; the diameter of the magnetic flux tube is set proportional to the magnetic field strength. We start with a 2D simulation in Cartesian coordinates $X \times Y$. Increasing the height of a box in Z direction, we compare the reconnection rates and other interesting quantities in the flow.

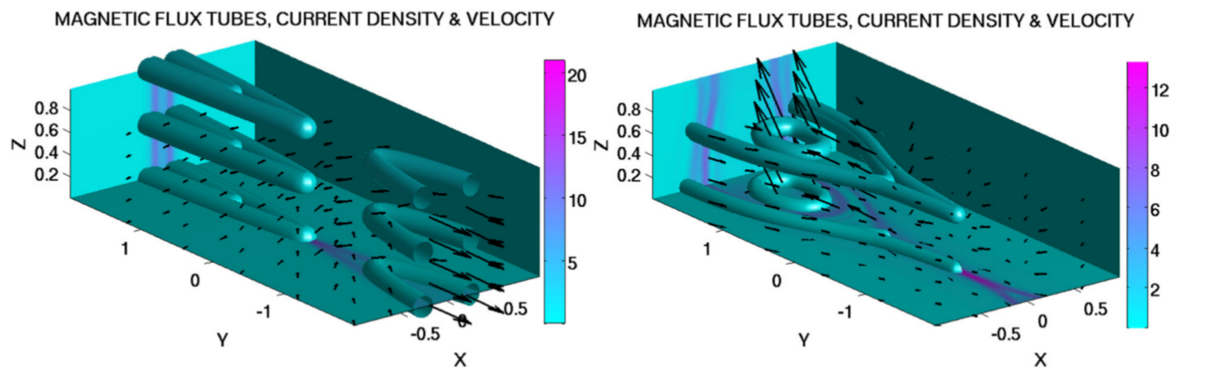

FIG. 3. Solutions in 3D in the first case, without the asymmetry in resistivity in the Z direction at T = 30 (left panel), and in the second case, with the asymmetry in the Z direction at T = 70 (right panel). Color grading is showing the toroidal current density at the boundary planes; tubes show a choice of the magnetic flux tubes, with the diameter of the tube set proportional to the magnetic field strength; arrows show velocity. A change in connectivity of the magnetic flux tubes in 3D, triggered by the asymmetry in resistivity in the vertical plane, additionally changes, and complicates, the topology of magnetic field.

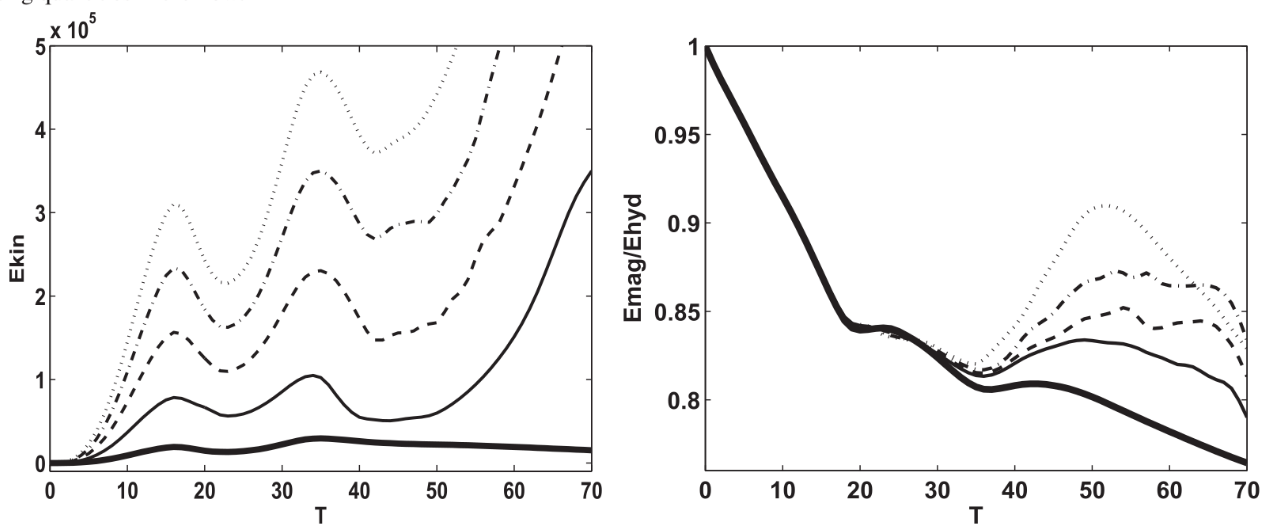

FIG. 4. Time dependence of the energy with different heights of the computational box in our simulations with reconnection in all three directions. In the left panel is shown the kinetic energy, and in the right panel is shown the ratio of magnetic to the sum of internal and kinetic energy. Results with different heights of the box h = 1, 2, 3, and 4, are shown in solid, dashed, dotted-dashed, and dotted lines, respectively. In thick solid line is shown the result with height h = 0.25 in the case with reconnection only in the X-Y plane, which is our reference 2D case. Kinetic energy during the build-up of reconnection is linearly increasing with height of the computational box, with the factor of proportionality about 2. The fraction of magnetic energy is steadily decreasing with time, until the reconnection in the third direction starts; then it increases proportionally with height.

Toy model: Orszag & Tang vortex

-authors study the properties of reconnection and formation of plasmoids in current sheets in an Orszag-Tang vortex (1979). They also determine the required resolutions to capture the full process of plasmoid formation.

-a flat spacetime Minkowski metric is assumed, relativistic ideal gas with an adiabatic index $\gamma = 4/3$, $p=10$ initial uniform pressure and rest mass density $\rho=1$. Using $\mathbf{B}=\nabla \times \mathbf{A}$ magnetic field is obtained from vector potential $\mathbf{A}=(0,0,A_z)$ on 2.5D Cartesian grid, such that $A_z=[\cos(2x)+\cos(y)]/2$, with the initial velocity $\mathbf{V}=(V_x,V_y,0)$, with $V_{max}=0.99/\sqrt{2}$, $V_x=-V_{max}\sin(y)$, $V_y=-V_{max}\sin(x)$. Electric field is initialized with $\mathbf{E}=-\mathbf{V}\times\mathbf{B}/c$. Minimum value of the gas-to-magnetic-pressure ratio is then $\beta=2p/B^2=10$ and max. magnetization $\sigma=B^2/(\rho h)\sim0.05$, with specific enthalpy $h=1+4p/\rho$.

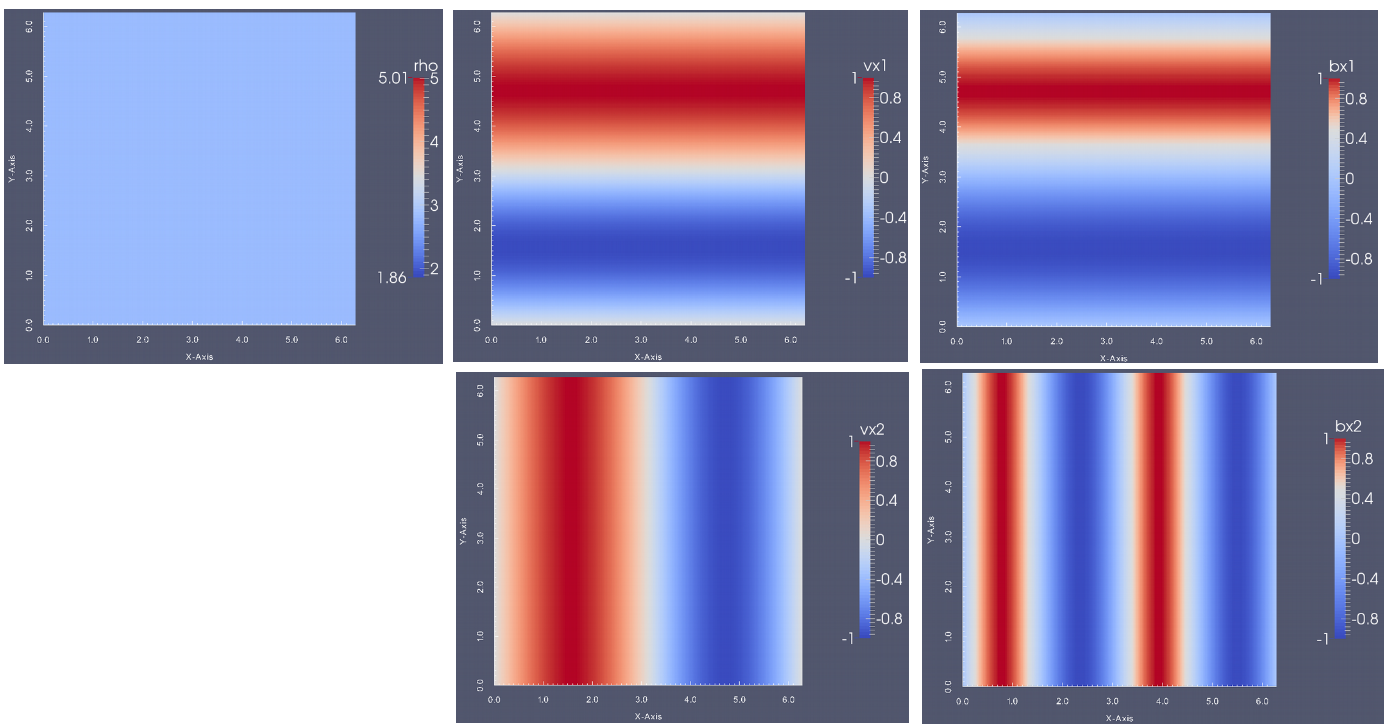

Initially: four alternating X-points and magnetic nulls, resulting in two magnetic islands along $y = 0$, $y = \pi$, and $y = 2\pi$. The vortex motion results in diagonal current sheets, which are compressed, and, depending on the S_L, can become tearing unstable and break-up in plasmoids.

Toy model

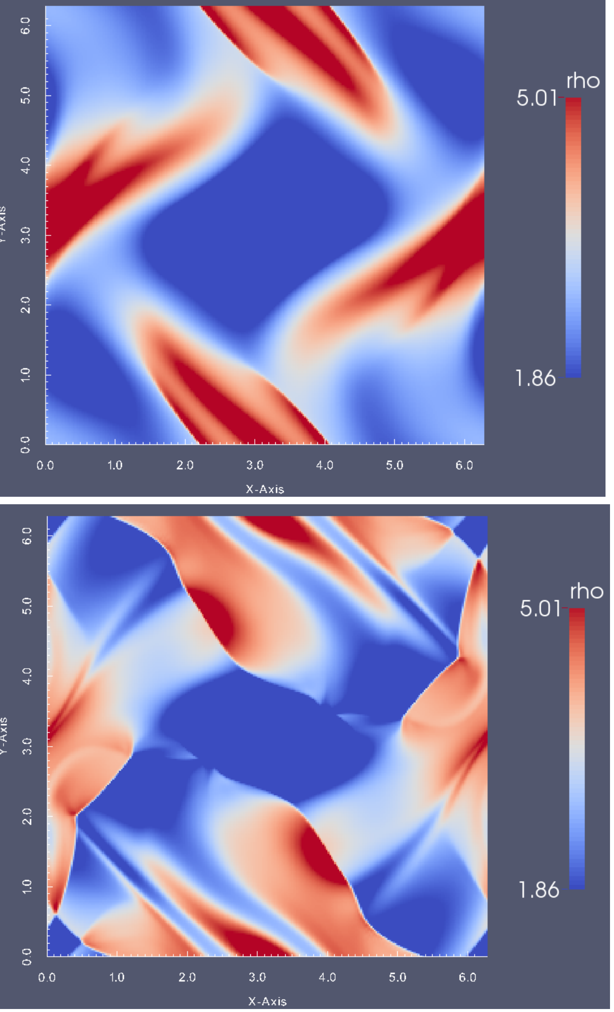

Basic resolution 128^2 cells in $x,y \in [0,2\pi]$ is used, with periodic b.c., which is then increased by AMR, in each level quadrupling the (effective) resolution, to study the convergence of the numerical solution (effective=total number of cells if the highest level is used, the actual number of cells is smaller). Simulations run to final time $t = 10t_c$, with $t_c = L/c$ the light-crossing time, where $L = 1$ is the typical length scale of the system.

Density in the next steps in the simulation.

A parameter study is performed, with a set of uniform and constant resistivities: $\eta \in [0, 10^{-5}, 2.5\times10^{-5}, 5\times10^{-5}, 10^{-4}, 5\times10^{-4}, 10^{-3}, 5\times 10^{-3}]$, chosen such that the corresponding Lundquist numbers $S = Lc/\eta \in [\infty, 10^5, 4\times10^4, 2\times10^4, 10^4, 2\times10^3, 10^3, 2\times10^2]$ range from infinity (ideal GRMHD) to well above and below the threshold for plasmoid formation $S_{th} \approx 10^4$.

Toy model

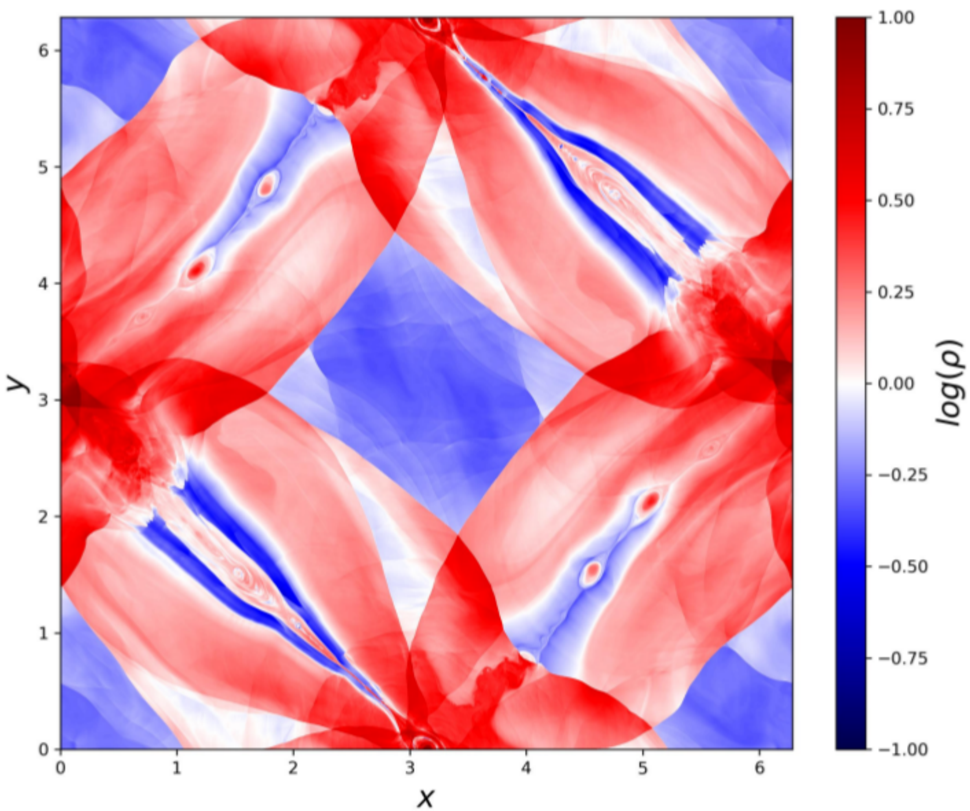

-For $S \geq 10^4$ the current sheets shrink until they become plasmoid-unstable. In the figure is shown the rest mass density ρ for $S = 10^5$ at $t = 10t_c$, where plasmoids are recognized as over-dense blobs of plasma in the thin current sheets. The current sheet is characterized by an anti-parallel magnetic field configuration resulting in a large out-of-plane component of the current density in the fluid frame. For lower Lundquist numbers $S < 10^4$ the current sheet does not become thin enough for the plasmoid instability to grow (e.g. left panel of figure in the next slide, for $S = 2 \times 10^3$ and resolution 8192^2).

They claim converged results if the evolution of the domain-averaged magnetic energy density $\bar{B}^2 \equiv \frac{\iint_V B^2 dxdy}{\iint_V dxdy}$ does not change anymore between successive doubling of the number of grid cells per direction over the full domain V

Toy model

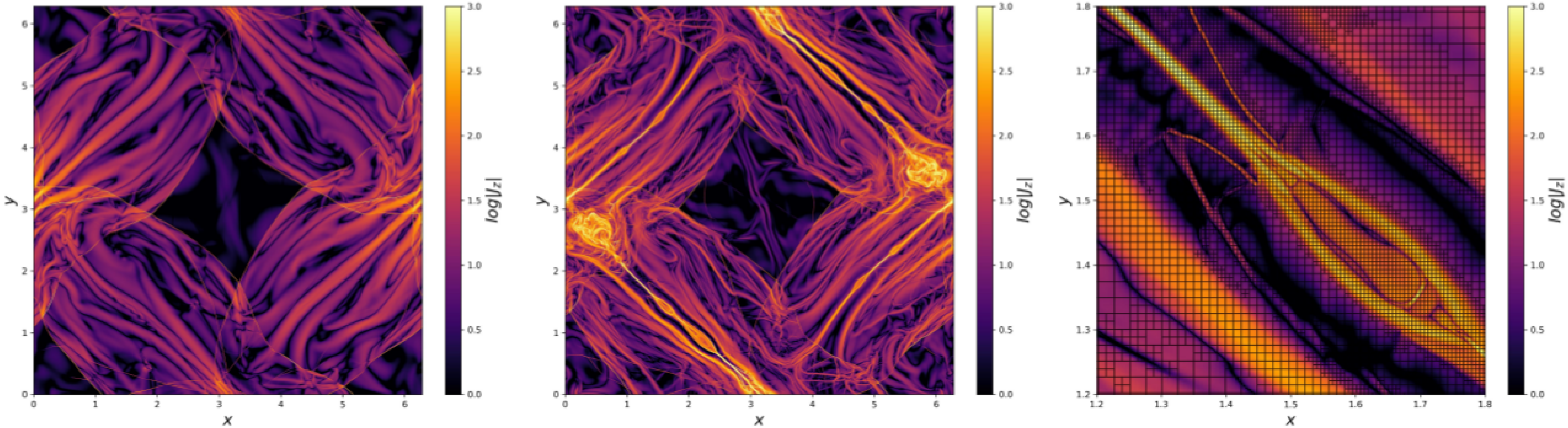

Figure 2. Logarithm of the out-of-plane current density magnitude $|J_z|$ at $t = 10t_c$ for $S = 2 \times 10^3$ (left), $S = 2 \times 10^4$ (middle), and a zoom into the current sheet for $S = 2 \times 10^4$ showing the AMR grid blocks (right), each consisting of 8×8 cells, in black. Both cases have an effective resolution of 8192^2 cells in the domain. The plasmoid-unstable current sheet on the right is captured by more than ten cells over its width.

The current sheet is characterized by an anti-parallel magnetic field configuration resulting in a large out-of-plane component of the current density in the fluid frame. For lower Lundquist numbers $S < 10^4$ the current sheet does not become thin enough for the plasmoid instability to grow (e.g. left panel of Figure 2 for $S = 2 \times 10^3$ and resolution 8192^2). $\mathbf{J} = \Gamma[\mathbf{E} + \mathbf{v} \times \mathbf{B}/c - (\mathbf{E} \cdot \mathbf{v})\mathbf{v}/c^2]/\eta$

Toy model

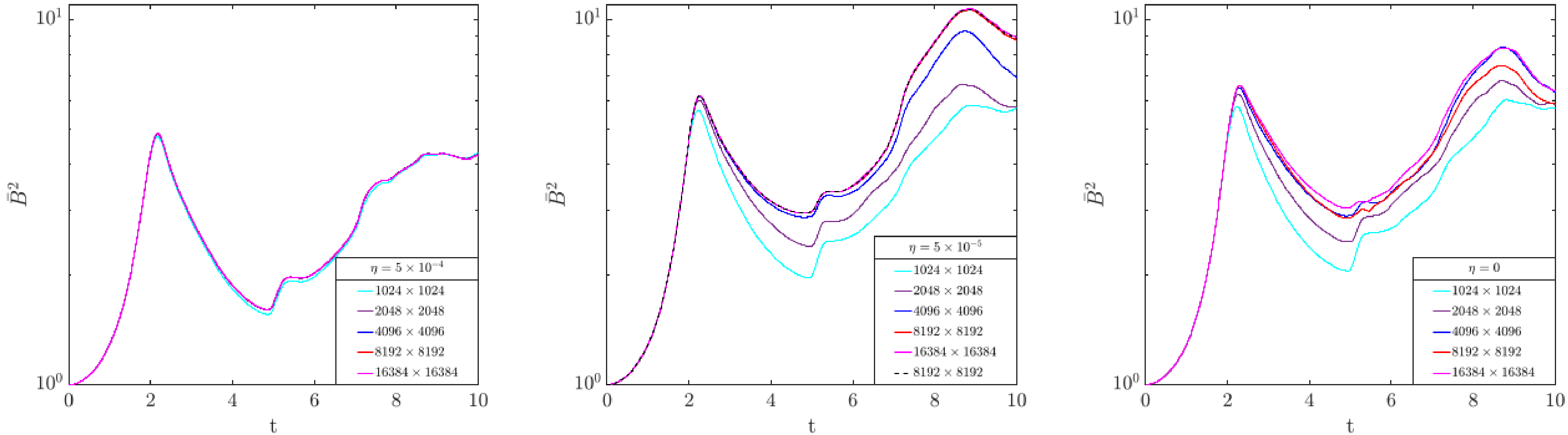

Figure 3. Evolution of the domain-averaged magnetic energy density $\bar{B}^2$ for $S = 2 \times 10^3$ (left), $S = 2 \times 10^4$ (middle), and the ideal case $\eta = 0$ (right) for all resolutions considered.

-For $S = 2 \times 10^4$ there are no visual differences between runs with resolutions of 8192^2 and 16384^2 grid cells (see middle panel). For resolutions < 8192^2 the (average) magnetic energy density is underestimated (more after t = 2tc) and the dissipation is governed by numerical resistivity that is larger than the explicit resistivity $\eta = 5 \times 10^{-5}$ affecting the energetics, heating, and plasmoid statistics.

-The effect of the AMR on the evolution of B^2 for $S = 2 \times 10^4$ is negligible compared to a (much costlier!) run with uniform resolution of 8192^2 grid cells (see the dashed black line in the middle panel).

-In ideal GRMHD ($\eta = 0$) run (left panel) is shown that in this case the magnetic energy density evolution (and also the numerical dissipation and heating of the plasma), does not converge even for the highest resolutions. Without resistive dissipation scale set by $\eta > 0$ the current sheet shrinks to the grid scale, and is captured by one grid cell over its width for all resolutions.

Reconnection rate

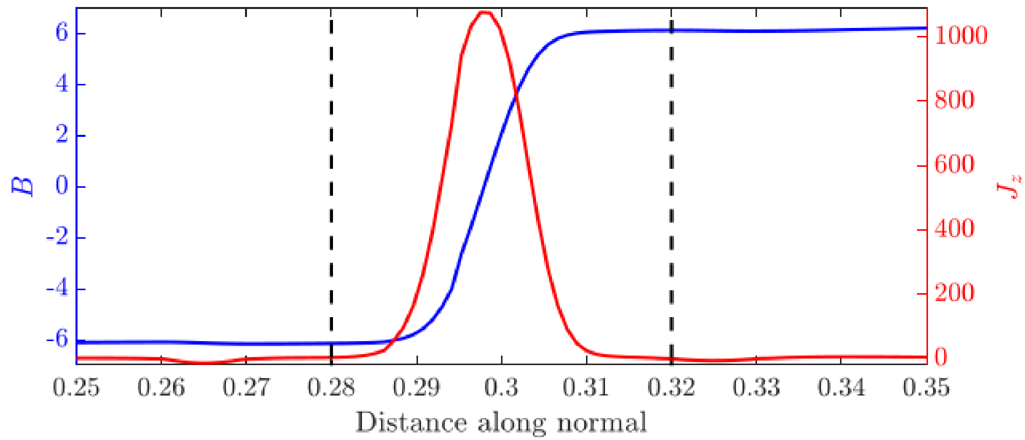

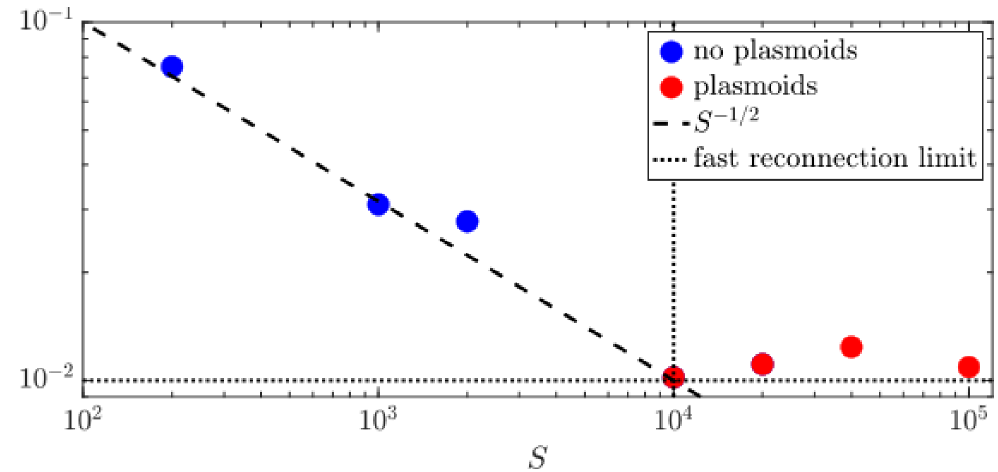

Analysis of the reconnection rate is done by measuring the inflow velocity into the current sheet. For the inflow speed determination, the upstream **E** × **B**-velocity is taken, with Vup /c = Ez,up /Bup . Five slices across the current sheet are taken (ensuring that the slice does not cut across a plasmoid) at t = 10tc for all cases with resolutions of 16384^2 such that even the thinnest sheet for S = 10^5 is resolved. Profile of Bup is taken by projecting the magnetic field along the current sheet and the location where the profile becomes flat is found (see the right panel for S = 2 × 10^4). Both the upstream electric and magnetic fields are averaged over 5 locations in the upstream on the slices on both sides of the sheet. The bulk flow velocity (v_bulk<<c such that Γ bulk = 1, where Γ=(1 − v^2 /c^2)^−1/2) of the vortex is accounted for by defining the speed on the left of the sheet as Vup,left /c = (Vbulk + Vin)/c and on the right of the sheet as Vup,right/c = (Vbulk − Vin)/c, such that Vrec/c = (Vup,left − Vup,right)/2c. Assuming that the outflow Vout = VA ≈ c, it gives the reconnection rate Vrec /c = Vin /Vout = Vin /c. Locally, in the upstream region of the current sheet, σ = B^2/(ρh) ≈ 8 such that the Alfvén speed around the sheet is VA = c[σ/(σ + 1)]^1/2 ≈ c and that the reconnection is relativistic. In the right panel we observe a Sweet-Parker scaling Vrec /c ∼ S ^−1/2 for S < 10^{-4} (blue circles and dashed black line) and plasmoid-dominated “fast” reconnection with a rate independent of the Lundquist number of Vrec /c ≈ 0.01 for S ≥ 10^4 (red circles and the dotted black line).

Reconnection in BH accretion flows

-It is much harder to localize and track the formation of current sheets in realistic BH accretion flows because of more complicated dynamics, and turbulence induced by the MRI. Accretion flows and current sheets depend on the magnetic field geometry.
-They model an accretion disk around a rotating black hole varying the initial conditions to study current sheet formation in different scenarios of magnetic field geometry.
-In the Magnetically Arrested Disk (MAD) scenario the MRI and subsequent turbulence in the inner accretion disk are suppressed due to large-scale magnetic flux. In axisymmetric simulations considered here, the arrested inflow is regularly broken by frequent bursts of accretion, allowing for a macroscopic equatorial current sheet to form and break in a periodic fashion. In a full 3D setup magnetically buoyant structures are interchanged with less-magnetized dense fluid resulting in a magnetic Rayleigh-Taylor instability, potentially sourcing interchange-type magnetic reconnection.
-In the Standard And Normal Evolution (SANE) state a fully turbulent accretion disk can develop due to a smaller magnetic flux and current sheets can form and interact with the turbulent flow
-Polarized synchrotron radiation observed by the Event Horizon Telescope (EHT) can probe the field line structure at event-horizon scales and put tighter constraints on the magnetization and inform us if accretion is in a SANE or a MAD state.
-Here both SANE and MAD scenarios are considered, studying whether forming current sheets can become tearing-unstable and produce macroscopic plasmoids before breaking up.

Simulations - setup

-Both MAD and SANE magnetic field configurations are cosnidered, around a Kerr black hole with a near extremal dimensionless spin a = 0.9375. Geometrized units are used, with gravitional constant, black-hole mass, and speed of light G = M = c = 1; then lengths scales are normalized to the gravitational radius $r_g = GM/c^2$ and times are given in units of r_g/c. Kerr-Schild coordinates are employed, with (r,θ,φ) radial, poloidal and toroidal angular coordinates, and time t. Simulations start from a torus in hydrodynamic equilibrium (Fishbone & Moncrief 1976) threaded by a single weak poloidal magnetic field loop, defined by the vector potential $A_\varphi \propto \max(q, 0)$, with q set to obtain a large torus resulting in a MAD state:

$$q = \frac{\rho}{\rho_{\rm max}}\left(\frac{r}{r_{\rm in}}\right)^3 \sin^3\theta \exp\left(-\frac{r}{400}\right) - 0.2,$$

$r_{in} = 20r_g$ and the density maximum ρ_{max} is located at $r_{max} = 41r_g$.

For SANE state, smaller torus is set with $r_{in} = 6r_g$ with ρ_{max} located at $r_{max} = 11r_g$.

$$q = \frac{\rho}{\rho_{\rm max}} - 0.2,$$

Plasma-β and the magnetization $\sigma = b^2/\rho$ for a cold (i.e., $p << \rho$) plasma are defined, using the magnetic field strength b^2 co-moving with the fluid:

Comoving E and B

Finally, it is useful to introduce the fluid-frame (comoving) electric and magnetic field (Bucciantini & Del Zanna 2013),

$$e^{\mu} = \Gamma(E^{i}v_{i})n^{\mu} + \Gamma(E^{\mu} + \gamma^{-1/2}\eta^{\mu\nu\lambda}v_{\nu}B_{\lambda}), \qquad (35)$$

$$b^{\mu} = \Gamma(B^{i}v_{i})n^{\mu} + \Gamma(B^{\mu} - \gamma^{-1/2}\eta^{\mu\nu\lambda}v_{\nu}E_{\lambda}), \qquad (36)$$

allowing to rewrite the electromagnetic part $T^{\mu\nu}_{\mathrm{EM}}$ of Equation (12) as (Qian et al. 2017),

$$\begin{aligned} T^{\mu\nu}_{\mathrm{EM}} = (b^2 + e^2)\left(u^{\mu}u^{\nu} + \frac{1}{2}g^{\mu\nu}\right) - b^{\mu}b^{\nu} - e^{\mu}e^{\nu} \\ - u_{\lambda}e_{\beta}b_{\kappa}(u^{\mu}\gamma^{-1/2}\eta^{\nu\lambda\beta\kappa} + u^{\nu}\gamma^{-1/2}\eta^{\mu\lambda\beta\kappa}). \end{aligned} \qquad (37)$$

The comoving electric and magnetic field strength, $e^2 := e^{\mu}e_{\mu}$, $b^2 := b^{\mu}b_{\mu}$, are also employed in the definition of useful dimensionless plasma quantities (e.g., the magnetization $\sigma_{\mathrm{mag}} := b^2/\rho$ and the gas-to-magnetic pressure ratio, or plasma-$\beta_{\mathrm{th}} := p_{\mathrm{gas}}/p_{\mathrm{mag}} = 2p/b^2$).

Simulations-setup

-Atmospheric rest-mass density and pressure are set as $\rho_{atm} = \rho_{min}$ r^−3/2 and $p_{atm} = p_{min}$ r^−5/2 where $\rho_{min} = 10^{-4}$ and p_{min} = 10^−6 /3. Floors on rest-mass density, pressure, and Lorentz factor $\Gamma < \Gamma max = 20$ are such that the magnetization $\sigma = b^2/\rho < \sigma\ max = 100$ and β^−1 = $b^2 /2p < \beta max= (10\sigma\ max)\ (\hat{\gamma}-1)$. Used is equation of state for a relativistic ideal gas with an adiabatic index of $\hat{\gamma} = 4/3$. The equilibrium fluid pressure is perturbed to trigger the MRI as $p = p_{eq}\ (1+Xp)$ with a random variable uniformly distributed between $Xp \in [-0.02; 0.02]$.

Dissipation in the flow is set by assuming small uniform constant resistivity $\eta=5 \times 10^{-5}$, giving large Lundquist number $S = r_g\ c/\eta = 2 \times 10^4$, well above the plasmoid threshold (the Schwarzschild radius r_g is taken as the typical length scale, and the speed of light c as the typical velocity). With small resistivity one can capture both ideal-MHD and the fast reconnection resulting in plasmoid formation in localized thin current sheets.

Simulations-results

-Both MAD and SANE configurations in ideal and resistive runs reach a quasi-steady-state, after approximately 2500rg/c and 500rg/c. It is measured by computing the magnetic flux through the horizon:
(g is the metric determinant)

$$\dot{\Phi} := \frac{1}{2}\int_0^{2\pi}\int_0^{\pi} |B^r|\sqrt{-g}\,d\theta d\phi,$$

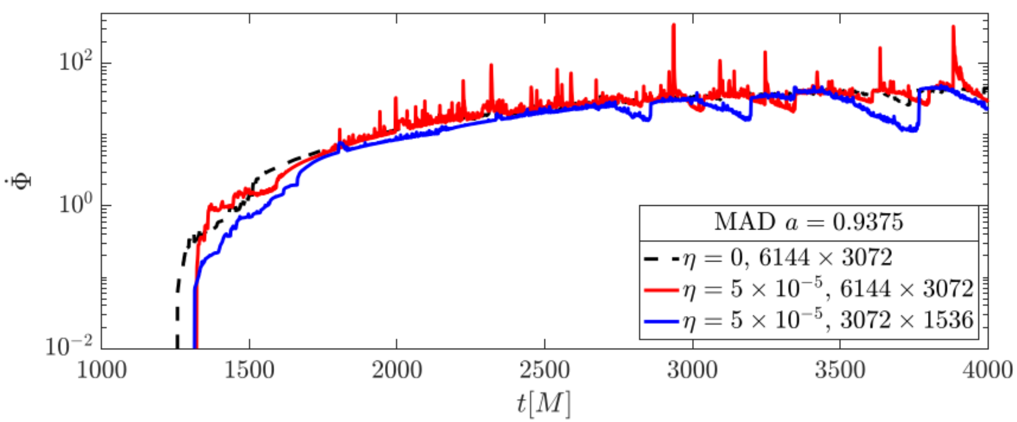

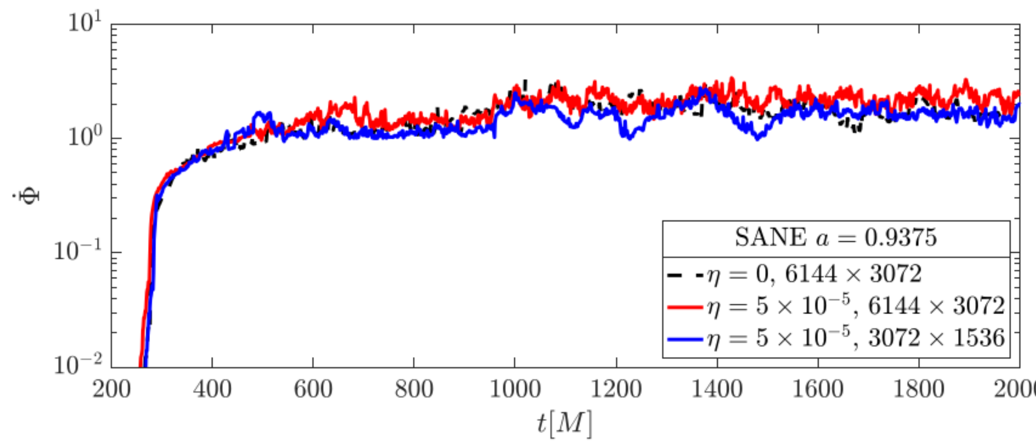

Time evolution for $\eta = 0$ (dashed black lines) and $\eta = 5 \times 10^{-5}$ (solid red lines) in MAD and SANE runs. The ideal and resistive results at a resolution of 6144×3072 are in agreement and the global accretion dynamics are unaffected by resistivity. With a resistive run at a twice smaller resolution per direction, 3072 × 1536 (blue lines) is shown convergence of the global accretion dynamics.

Simulations-SANE results

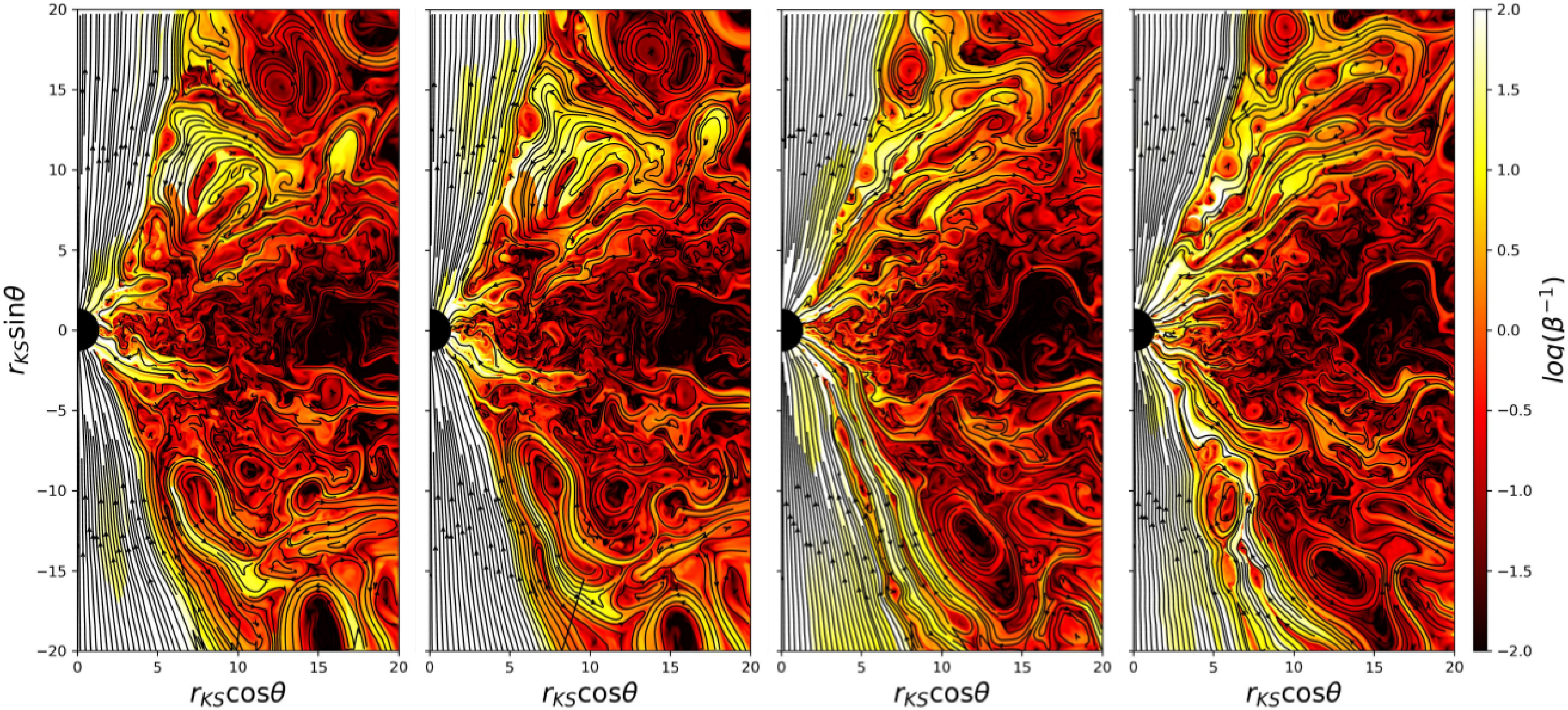

Figure 6. $\beta^{-1} = b^2/(2p)$ at four typical times $t = [1460, 1480, 1540, 1580]r_g/c$ (from left to right) during quasi-state-state phase of accretion in the SANE configuration. Magnetic field lines plotted are on top as solid black lines. In the bottom half one can detect the accretion of a magnetic flux tube at $r_{KS}\cos\theta = x \approx 6r_g, r_{KS}\sin\theta = y \approx -8r_g$ (left two panels) that inflates, opens up and becomes tearing unstable (third panel) after it connects to the black hole, and produces copious plasmoids coalescing into large-scale structures at $x \approx 5r_g, y \approx= -10r_g$ (fourth panel) with a typical size of about one Schwarzschild radius. In the top half of the panels a similar process can be seen at $x \approx 7r_g, y \approx 13r_g$ in the second and third panel, also resulting in a large-scale plasmoid at $x \approx 9r_g, y \approx 18r_g$ in the fourth panel.

Simulations-SANE results

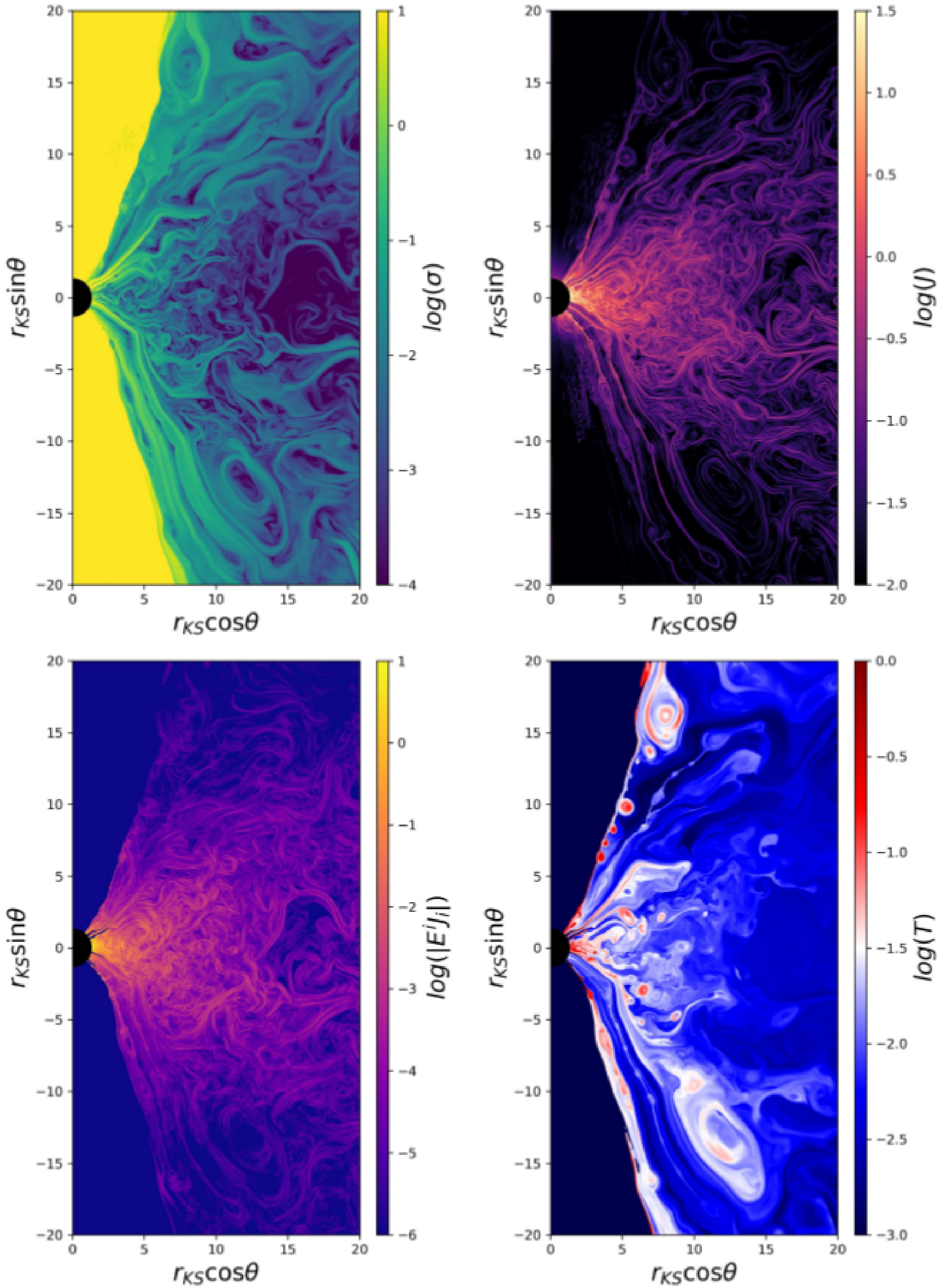

SANE quasi-steady-state phase of accretion at t = 1540rg /c. Top left: Magnetization σ showing that current sheets along the jet's sheath are in the relativistic regime σ >> 1, whereas in the disk they are in the transrelativistic regime σ ≲ 1. Top right: The thin tearing-unstable reconnection layers are indicated by a strong current density. Bottom left: Plasmoids in the current sheets are heated by Ohmic heating close to the event horizon. The strong parallel electric field indicated by E^iJ_i can accelerate particles to non-thermal energies. Bottom right: Plasmoids both in the disk and along the jet's sheath are heated up to relativistic temperatures T = p/ρ ∼ 1.

Simulations-SANE results

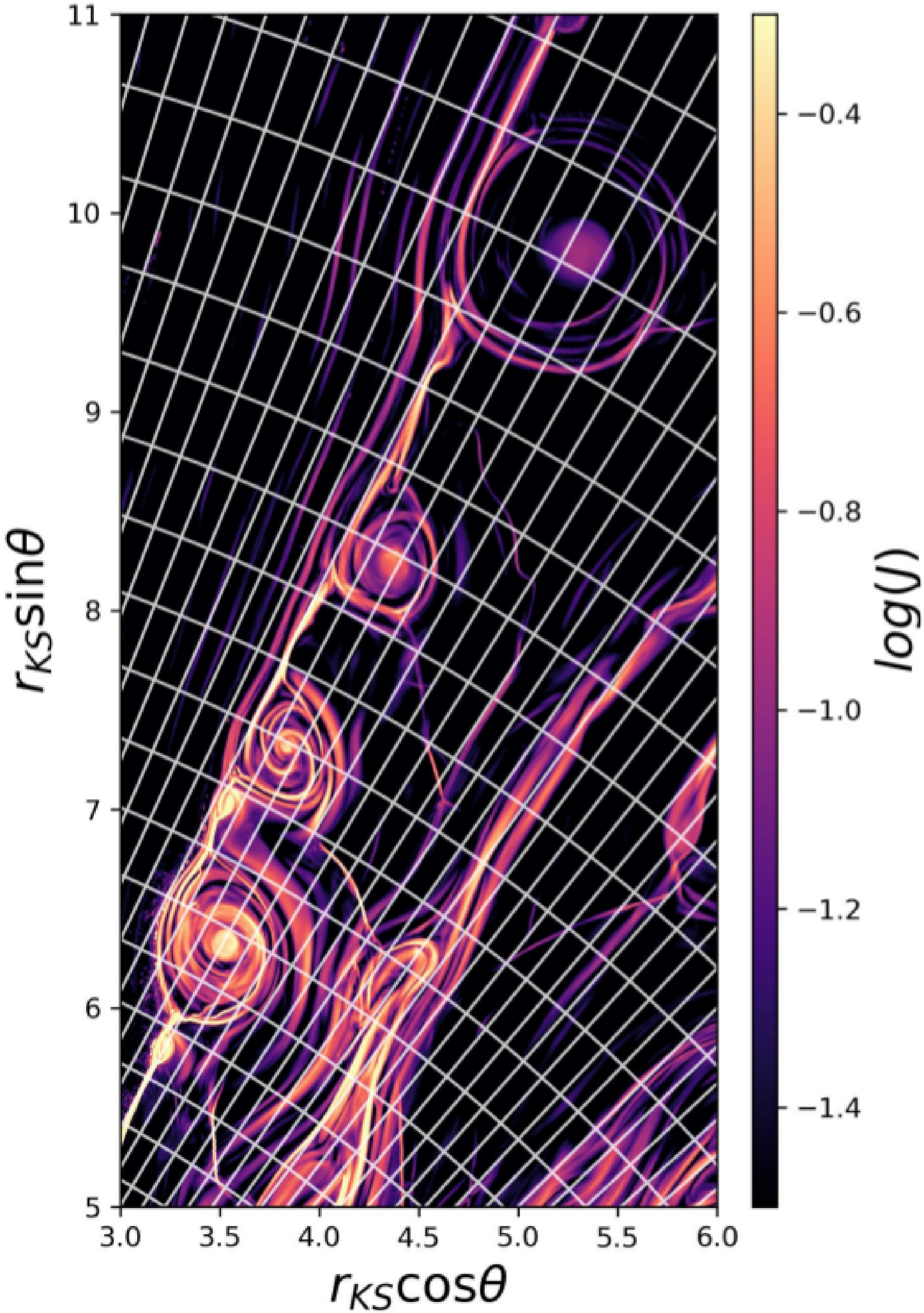

Zoom into a current sheet (top-right panel above): plasmoids are advected along the jet's sheath, reaching a typical size of the order of a few Schwarzschild radii through coalescence. The on-plotted grid-block structure (white rectangles) shows that each current sheet is captured by approximately 10 cells over its width. Each block represents 64 × 32 cells.

The strong parallel electric field indicated by $E^i J_i$ in the bottom left panel can potentially accelerate particles to non-thermal energies.

Simulations-MAD results

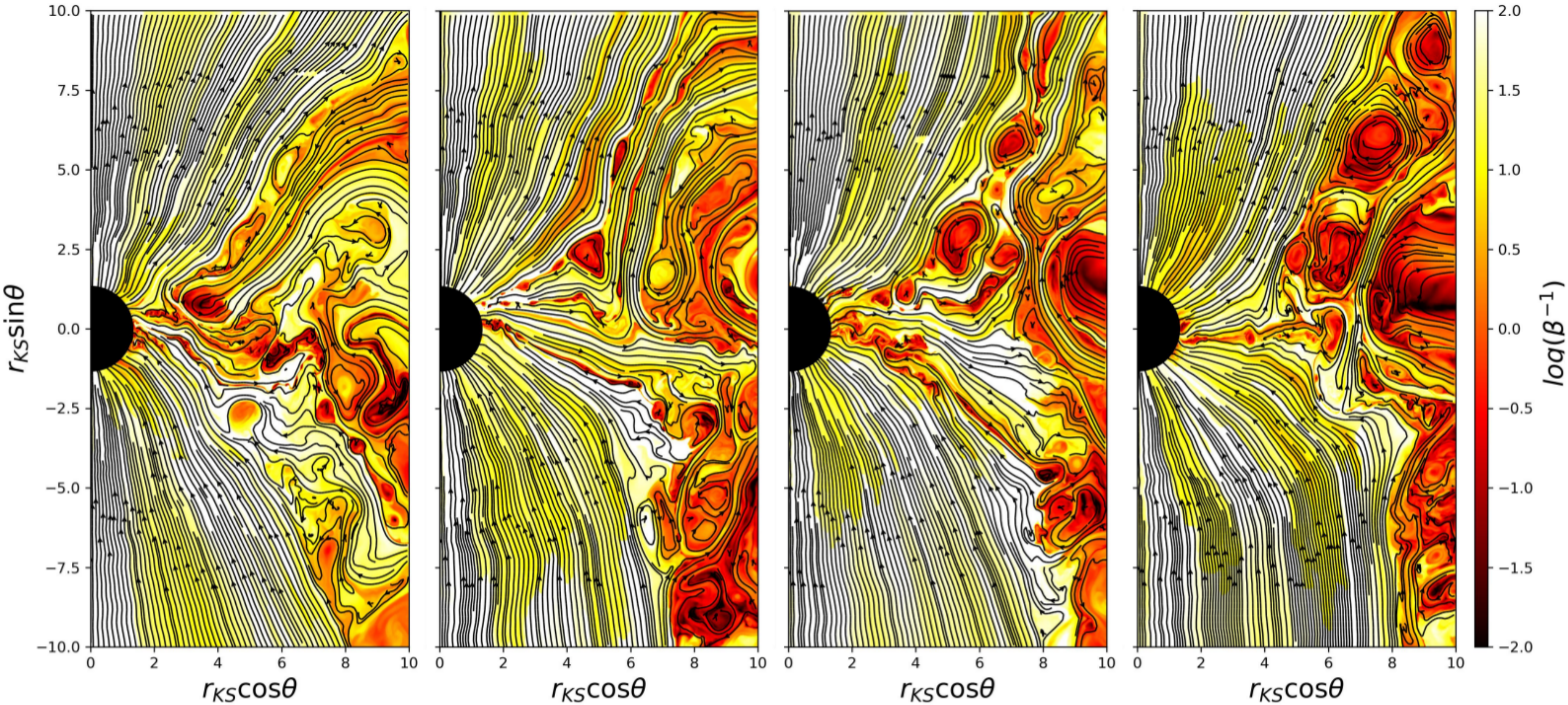

Figure 9. $\beta^{-1} = b^2/(2p)$ at four typical times $t = [2941, 2971, 2988, 3009]r_g/c$ (from left to right) during the quasi-state-state phase of accretion in the MAD configuration. Magnetic field lines are plotted on top as solid black lines. In the top half one can detect the accretion of a magnetic flux tube (left panel) at $x \approx 3r_g, y \approx 1r_g$ that opens up and becomes tearing unstable (second panel) after it connects to the black hole, and produces copious plasmoids coalescing into large-scale structures (third and fourth panel) at $x \approx 5r_g, y \approx 2.5r_g$ with a typical size of about one Schwarzschild radius.

Simulations-MAD results

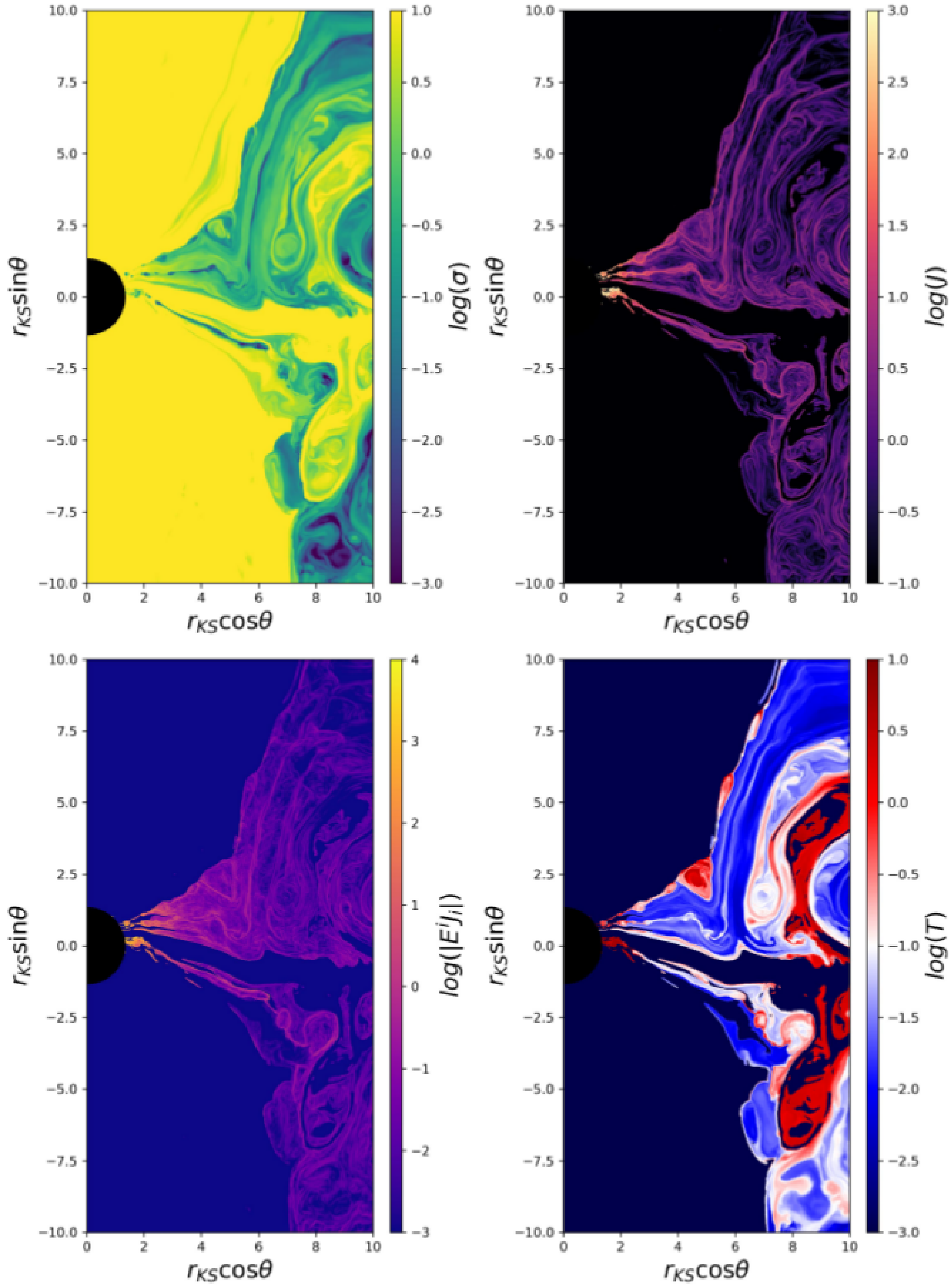

MAD, quasi-steady-state at t = 2971rg/c. Top left: Magnetization σ showing that current sheets close to the event horizon are in the relativistic regime σ>>. Top right: The thin tearing-unstable reconnection layers are indicated by a strong current density. Bottom left: Plasmoids in the current sheets are heated by Ohmic heating close to the event horizon. Bottom right: Plasmoids formed in the equatorial sheets are advected into both the disk and along the jet's sheath and are heated up to relativistic temperatures $T = p/\rho \sim 10$, an order of magnitude larger than in the SANE case.

Simulations-reconnection rates

The reconnection rates are computed in a similar way as for the Orszag-Tang vortex for both MAD and SANE configurations.

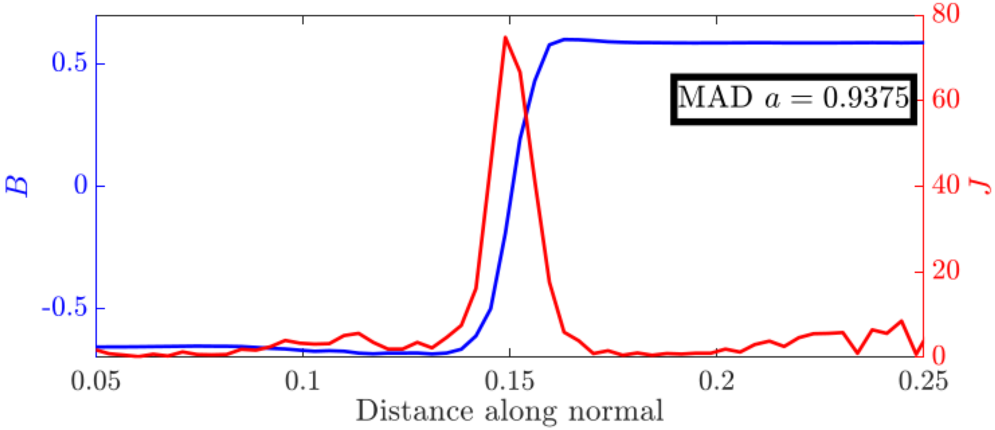

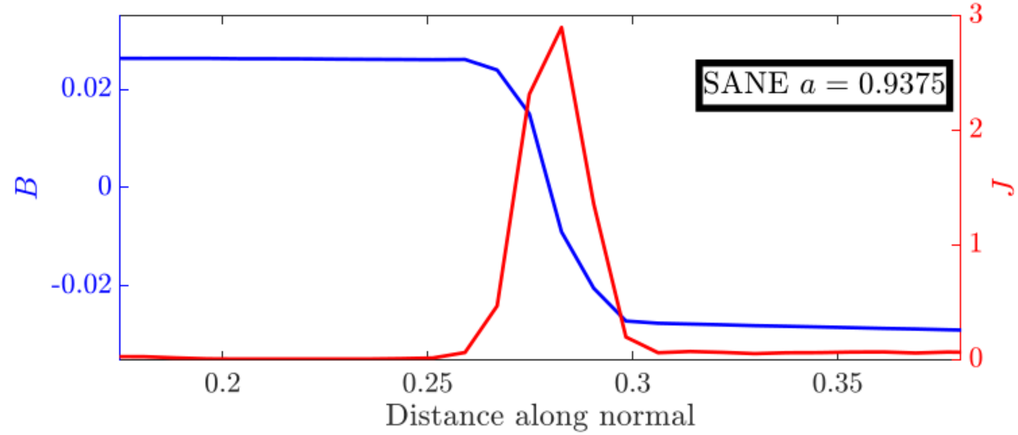

The fields are projected along the direction parallel to the current layer to determine the upstream geometry, and a typical Harris-type sheet structure is found, both for the magnetic field and the current density magnitude J. Three magnetic field components switch sign in the current sheets, indicating that reconnection occurs in both MAD and SANE cases. Inflow speed is determined from the E × B velocity projected along the direction perpendicular to the current sheet, and then calculated the reconnection rate as $V_{rec}/c = (V_{up,left} - V_{up,right})/2c$. In both MAD and SANE configurations they select ten current sheets at different times during the quasi-steady state phase of accretion and consistently find a reconnection rate between 0.01c and 0.03c. This is in accordance with analytic resistive MHD predictions for plasmoid-dominated reconnection in isolated current sheets.

Summary

General-relativistic resistive magnetohydrodynamics simulations were performed, to model magnetic reconnection and associated plasmoid formation in a wide range of accretion flows. An explicit resistivity allows for converged numerical solutions. The electromagnetic energy density evolution and dissipation become independent of the grid scale for the extreme resolutions in the study.

-authors show that plasmoids form due to magnetic reconnection in black-hole accretion flows, regardless of the initial size of the disk and the magnetization during the quasi-steady-state phase of accretion, in both MAD and SANE cases

-plasmoids form in current sheets close to the event horizon within 5 to 10 Schwarzschild radii, with the reconnection rates between 0.01c and 0.03c, consistent with studies of reconnection in isolated Harris-type current sheets. Plasmoids can then merge, grow to macroscopic scales of the order of a Schwarzschild radius, and are advected along the jet's sheath or into the disk. The largest plasmoids are energized to relativistic temperatures by magnetic reconnection and contribute to the heating of the jet's sheath.

-In the MAD case the magnetization is significantly higher close to the event horizon, powering hot spots with relativistic temperatures $T = p/\rho \sim 10$, an order of magnitude higher than in the SANE case $T \sim 1$.

Thank you